ACS OMEGA

http://pubs.acs.org/journal/acsodf

Article

Amperometric Hydrogen Sensor Based on Solid Polymer Electrolyte and Titanium Foam Electrode

Wanshuo Gao,[†] Zinan Zhi,[†] Shurui Fan,* Zhongqiu Hua,* Haoyi Li, Xuanyue Pan, Wentao Sun, and Huicheng Gao

Cite This: *ACS Omega* 2022, 7, 24895−24902

Read Online

ACCESS | Metrics & More | Article Recommendations | Supporting Information

ABSTRACT: Trace hydrogen detection plays an important role in the safety detection of lithium-ion batteries (LIBs) due to the generation and leakage of trace hydrogen in the early stage of LIBs damage. In this work, an amperometric hydrogen sensor based on solid polymer electrolyte was reported. The sandwich device structure was realized, which could directly diffuse the gas from both sides to the three-phase interface (gas/electrode/electrolyte) to participate in the reaction through the optimal design of the gas diffusion path. Then, platinum nanoparticles (Pt-NPs) were loaded on the metal foam by electroplating, and the porous electrode was filled with solid polymer electrolyte. A sensor with high specific surface area, high catalytic activity, and high sensitivity was obtained. Finally, the hydrogen oxidation reaction (HOR) mechanism of the platinum-loaded (Pt-loaded) titanium foam (Ti foam) electrode under both anaerobic and aerobic conditions was verified, and the properties of the sensor was evaluated. The hydrogen sensor with a "sandwich" structure has the advantages of high sensitivity, good stability, low detection limit and low cost, which provides a technical solution for the safety and real-time monitoring of LIBs.

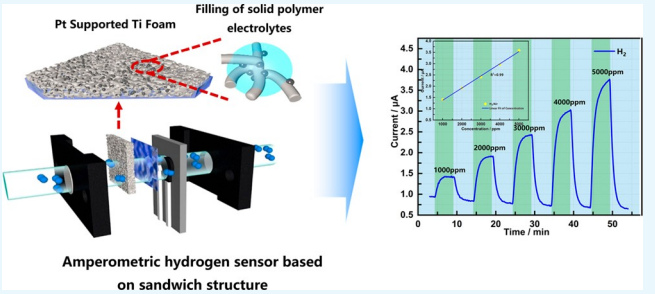

INTRODUCTION

Recently, the rise of intelligent wearable electronic devices used in life, medical treatment, and sports as well as the development of transportation power systems, aerospace, and other fields have promoted the wide application of lithium-ion bateries (LIBs).[1,2] However, the damage of LIBs often causes serious safety accidents in a short time, which means that it is necessary to detect the damage of LIBs as early as possible.[3−5] At the same time, it is worth mentioning that trace hydrogen detection is an effective means of LIBs safety monitoring. The reason is that the thermal runaway caused by the overcharge of LIBs generate a large number of lithium (Li) dendrites under high temperature conditions, which react with the organic electrode solution binder to generate gases such as hydrogen.[6−8] According to the study of Yuan et al., trace hydrogen detection can advance the alarm time to 639 s before the smoking of the LIBs, which preliminarily illustrates the feasibility of the scheme.[9]

Electrochemical gas sensors, especially amperometric gas sensors, are widely used in trace gas detection due to their advantages of high sensitivity, low manufacturing cost, environmental protection, low power consumption, and easy integration.[10−13] At the same time, combined with the international standards of hydrogen detection and the monitoring requirements of LIBs,[14−17] stricter requirements are put forward for the sensitivity, response speed, and anti-interference ability of hydrogen detection. Furthermore, it is necessary to use low-cost hydrogen sensors to rapidly detect trace hydrogen (ppm level) for the popularization of safety detection of LIBs.[18,19]

The design of the device structure is one of the key factors that determine the performance of the amperometric gas sensor. Recently, screen-printed electrodes (SPEs) based on room temperature ionic liquids (RTILs) have attracted extensive attention due to their simple structure, small size, and easy integration.[20] However, conventional electrode structures based on solid ceramic substrates have limited gas diffusion rates because gas needs to dissolve and diffuse in RTIL before reaching the three-phase interface. The difference is to use a porous ceramic substrate as the gas diffusion barrier to improve the sensor design as pointed out in our previous study.[21] The gas molecules directly diffuse from the porous substrate to the three-phase interface without passing through the electrolyte membrane, which effectively improves the response speed of the device. Besides, since the interface between the electrolyte membrane and the electrode is a two-dimensional planar structure, the area of the effective three-

Received: June 9, 2022
Accepted: June 21, 2022
Published: July 6, 2022

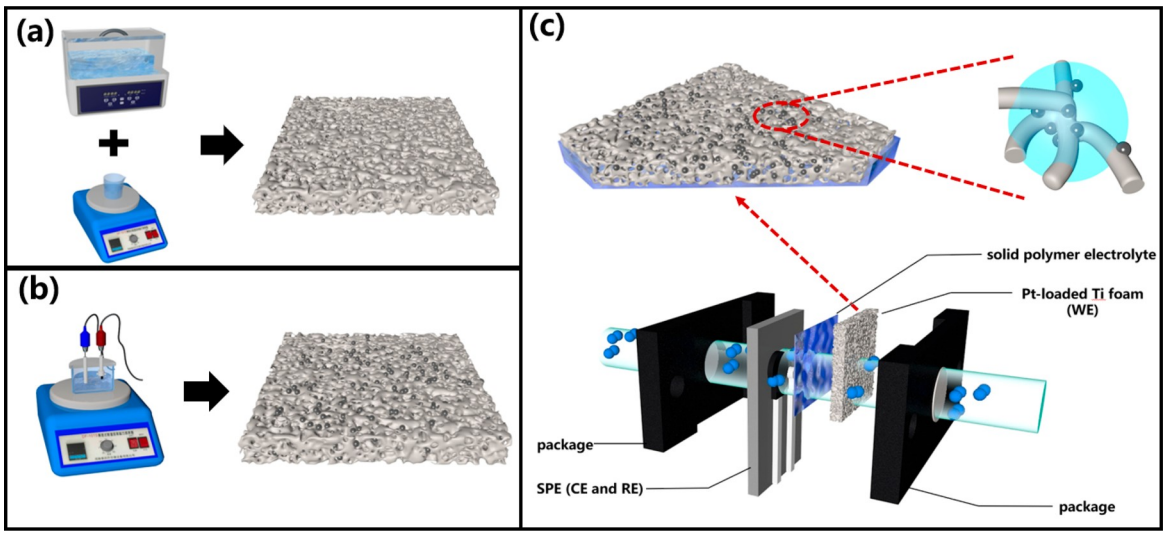

Figure 1. Process of Ti foam (a) pretreatment and (b) electroplating and (c) the illustration of the structure of the sensor.

phase interface is small, which limits the sensitivity of the hydrogen sensors. In contrast, traditional electrochemical gas sensors based on aqueous solutions of strong acids or alkalis have limited lifetimes and operating temperature ranges. However, the electrolyte solution and the porous electrode form the large three-phase interface, which ensures the high sensitivity of the sensor. In addition, it is worth mentioning that Korotcenkov et al. improved the "Clark" type gas sensor.[22] The working electrode (WE) was in direct contact with most of the electrolyte and in contact with air, and the mass transfer rate of hydrogen to the three-phase interface was faster. Then, Blurton et al. adopted fuel cell electrode technology and a gas diffusion electrode (GDE) for the design of the sensor.[23] Hydrogen diffused through the porous current collector directly to the three-phase interface, and the sensor can achieve a fast response, high sensitivity, and low detection limit. In conclusion, the performance of the sensor can be effectively improved by optimizing the gas diffusion path and increasing the contact area between the electrolyte and the electrode, which has reference significance for the design of the device structure.

In this study, a novel amperometric gas sensor was designed and fabricated with a metal foam as the electrode, which was filled with RTIL electrolyte simultaneously. This design enabled a very high specific surface area and a strong electrochemical activity when loaded with platinum nanoparticles (Pt-NPs). The sensor can realize the direct diffusion of gas from both sides to the three-phase interface to participate in the reaction. At the same time, the electrochemical behavior of hydrogen gas was explored in combination with a solid substrate sensor with a planar structure. It is believed that the present work could provide a fast hydrogen detection for LIBs safety monitoring.

2. EXPERIMENTAL SECTION

2.1. Reagents and Apparatus. The chemical reagents and the materials of the experiment used were chloroplatinic acid ($H_{14}Cl_6O_6Pt$, 99.9%, Shanghai Aladdin Biochemical Technology Co., Ltd.), hydrochloric acid (HCl, 12 M, purity ≥99.7%, Shanghai Aladdin Biochemical Technology Co., Ltd.), nitric acid (HNO_3, 0.1 M, Shanghai Aladdin Biochemical Technology Co., Ltd.), polyvinylidene fluoride resin (PVDF, molecular weight 1.1 × 10^6, Arkema, France), *N*,*N*-dimethylformamide (DMF, purity ≥99.8%, Shanghai Aladdin Biochemical Technology Co., Ltd.), titanium foam (Ti foam, purity ≥99 %, Yiminglong Electronic Materials Co., Ltd.). The types of RTIL used was 1-butyl-1-methylpyrrolidinium bis-(trifluoromethylsulfonyl)imide ([Bmpy][NTf_2], purity ≥99 %, Bailingwei Reagent Co., Ltd.). All experiments were performed at 298 ± 2 K without special instructions. The analytical gas followed the certified gas standards (Air Chemistry Co., Ltd., Beijing). The gas concentration required for the experiment is diluted with standard gas with nitrogen (purity ≥99.999%) or synthetic air (purity ≥99.999%) by mass flow controllers (MFC), where the setup for the characterization of sensor performance is shown in Figure S1. All of electrochemical measurements were carried out with the Electrochemical Workstation (Netherlands IVIUM Technologies B.V.). Field-emission-scanning electron microscopy and energy dispersive X-ray detection (FE-SEM and EDX, Zeiss Gemini Sigma 300), inductively coupled plasma emission spectrometry (ICP, Agilent ICPOES730), X-ray photoelectron spectroscopy (XPS, Thermo Escalab 250Xi), and X-ray diffraction (XRD, Bruker D8 Advance) was used to analyze the appearance and microstructure of the metal foam after platinum loading.

2.2. Electroplating Processes. Taking titanium foam (Ti foam) as an example, the experimental process of WE loaded by Pt was briefly described below. Ti foam (3.3 × 10 × 0.5 mm^3) was immersed in acetone and then sonicated for 10 min. Then, Ti foam was soaked in hydrochloric acid to remove the oxide film on the metal surface, according to Figure 1a. After pretreatment, Ti foam was stored in alcohol to prevent air oxidation. Next, the chloroplatinic acid particles were dissolved in a dilute nitric acid solution to obtain a plating solution with a pH of about 1. The type of acid solution used (inset in Figure S2b) and the selection of electroplating potential (Figure S2a) are detailed in the Supporting Information. The electrodes were cleaned with alcohol after electroplating at 343 K by a potentiostat (Figure 1b). The loading of Pt on Ti foam was controlled according to the amount of electricity transferred during the electroplating process.

2.3. Fabrication of Sensor Devices. Using [Bmpy]-[NTf_2], PVDF, and DMF as raw materials, the solidified liquid was prepared by melting and stirring with organic solvent. The

https://doi.org/10.1021/acsomega.2c03610
ACS Omega 2022, 7, 24895−24902

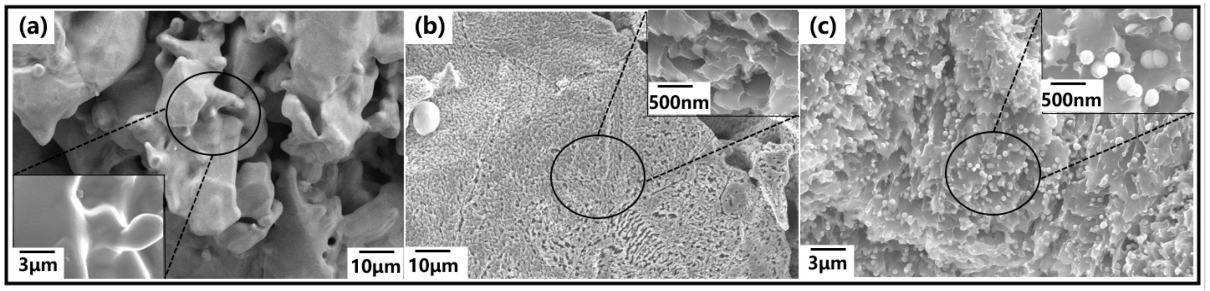

Figure 2. SEM images of Ti foam (a) before and (b) after pretreatment and (c) after electroplating.

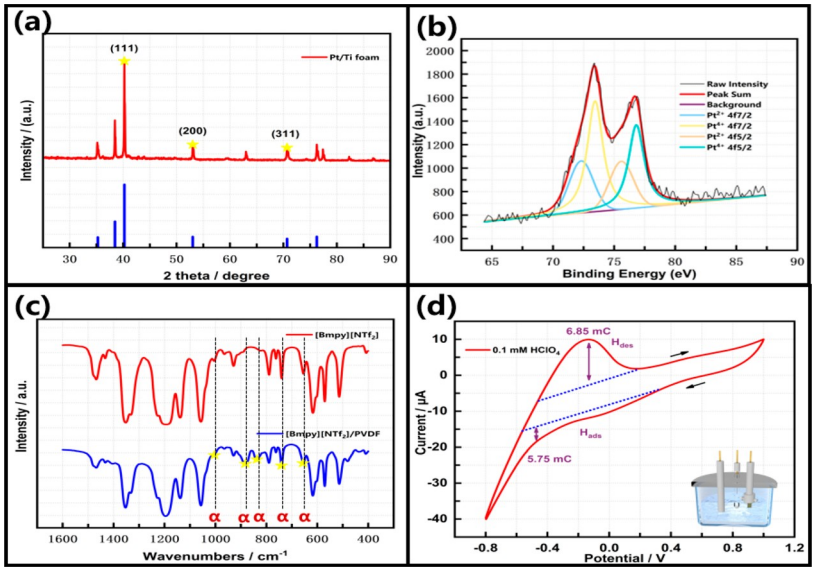

Figure 3. (a) XRD and (b) XPS analysis of Pt-loaded Ti foam, (c) FTIR of RTIL and solid polymer electrolyte, and (d) determination of hydrogen adsorption and desorption peaks in CV of Pt-loaded Ti foam in 0.1 mmol/L perchloric acid solution.

plated and dried Ti foam was placed in a petri dish and coated twice with the solidified liquid. The porous WE filled with solid polymer electrolyte was obtained after complete drying in an oven at 353 K and sintering at 473 K. CE and RE were made by screen-printing with a porous ceramic substrate. The 3D-printed package was designed for the device tightened Ti foam electrode and SPE, as shown in Figure 1c. At the same time, a solid polymer electrolyte film was spaced between the two layers of electrodes to prevent the solid polymer electrolyte and Ti foam from being completely coated, resulting in a short circuit between WE and RE. A more detailed sensor fabrication process is described in the Supporting Information.

RESULTS AND DISCUSSION

3.1. Material Characterization. Ti foam was treated with nitric acid to remove the oxide film on the surface. However, it was found that the surface of Ti foam was slightly corroded, compared with Ti foam without pretreatment as shown in Figure 2a,b. Meanwhile, Ti foam can be found with a pore size range from 70 to 100 μm. The specific surface area of Ti foam was increased by acid corrosion, which was beneficial for Pt plating. The size of the Pt-NPs was about 200 nm, which were evenly distributed on the surface of Ti foam without obvious agglomerations. As can be seen from Figure 2c, no continuous Pt film structure was formed. Therefore, the high specific surface area of Pt-NPs provided a large number of electrochemically active sites for the subsequent hydrogen oxidation reaction (HOR).

The Pt/Ti foam electrode was consistent with the pattern of Pt in the orthorhombic state (PDF no. 44-0003) and crystal structure and slightly different from the Pt in the metallic phase (PDF no. 04-0802), according to XRD patterns in Figure 3a. However, the XRD pattern indicated the possible presence of Pt in a combined state. Therefore, the chemical state of Pt on the Ti foam electrode was further investigated by XPS analysis. By peaks fitting to the data, the Pt^{2+} $4f_{7/2}$ peak at 72.4 eV and the Pt^{2+} $4f_{5/2}$ peak at 75.6 eV indicated the presence of PtO, and the Pt^{4+} $4f_{7/2}$ peak at 73.5 eV and the Pt^{4+} $4f_{5/2}$ peak at 76.7 eV indicated the presence of PtO_2, as shown in Figure 3b. It can be seen that most of the Pt present on Ti foam electrode was divalent and tetravalent. It was found that the RTIL ([Bmpy][NTf_2]) in the solid polymer electrolyte after high-temperature casting was not denatured according to FTIR of Figure 3c. It was found that the solid polymer electrolyte and RTIL are consistent with the characteristic peaks. According to the absorption peak of PVDF and the characteristic band of the α phase, it indicated that PVDF appeared as the α phase.

In our previous work, the large porosity of the porous ceramic was used as the substrate and the Pt SPE has a rough surface,[21,24] which results in a small three-phase interfacial area between the smooth solid polymer electrolyte membrane and WE. The Pt electrode layer with a thickness of 10 μm was formed, which led to a waste of precious metal. Bulk Pt

https://doi.org/10.1021/acsomega.2c03610
ACS Omega 2022, 7, 24895−24902

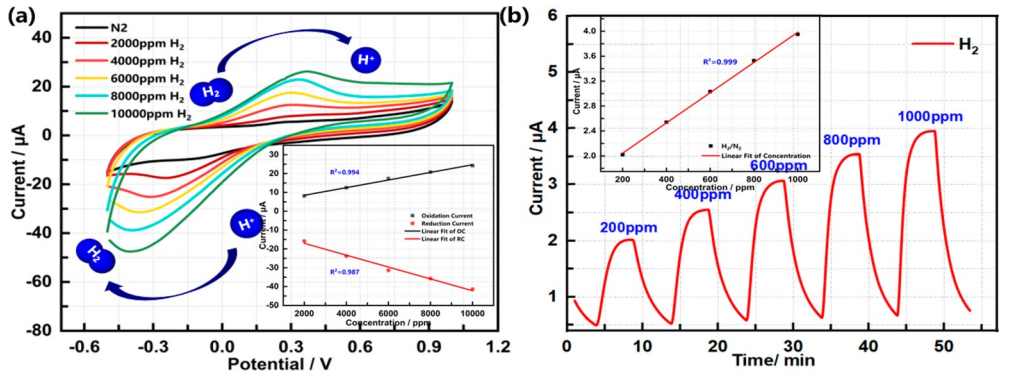

Figure 4. (a) CV of SPE at different hydrogen concentrations under anaerobic conditions, (b) chronoamperometry of the "sandwich" sensor at different hydrogen concentrations, and the insets are the linear fit of current and hydrogen concentration.

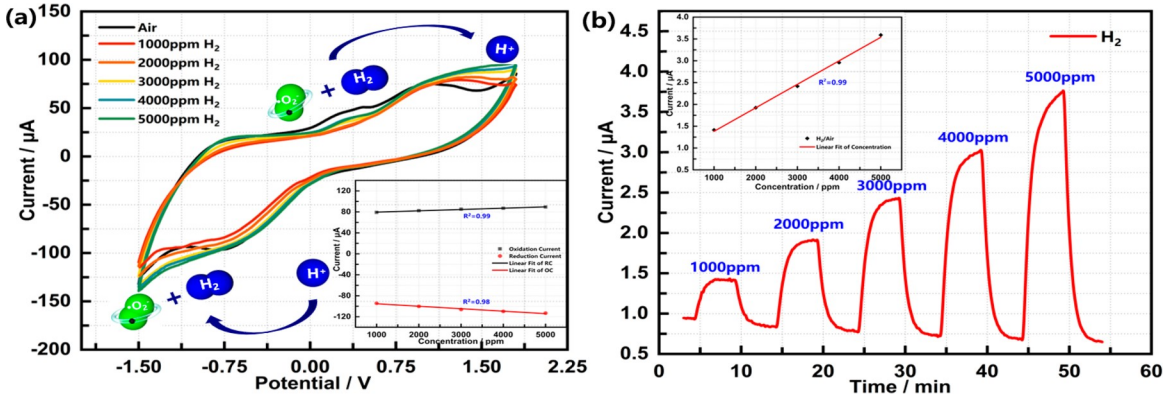

Figure 5. (a) CV for different hydrogen concentrations under aerobic conditions and (b) chronoamperometry at different hydrogen concentrations. The insets illustrate the linear fit of the chronoamperometry current to the hydrogen concentration.

electrodes not only increase the fabrication cost but also reduce the sensitivity of the sensor due to the small electrochemically active surface area (ECSA) and low catalytic efficiency. Conversely, the three-dimensional structure of the metal foam provides a high specific surface area for the loading of Pt-NPs. The ECSA of the material was characterized by CV in 0.1 mmol/L perchloric acid solution.[25,26] It found that the adsorption and desorption peaks of hydrogen appeared around −0.1 V, as shown in Figure 3d. The charges for the hydrogen adsorption and desorption processes were obtained by integration to be 6.85 mC and 5.75 mC. According to the formula

$$\mathrm{ECSA} = Q/C \quad (1)$$

Q is the electric quantity (unit, C), and C is the unit adsorption capacitance of Pt to hydrogen, which was a constant of 0.21 mC/cm^2. The resulting ECSA was 32.6 cm^2. It was shown that the Pt-supported Ti foam electrode had great electrochemical activity.

3.2. Sensing Properties of Hydrogen. [Bmpy][NTf$_2$] is more suitable as the electrolyte for HOR by comparing different RTILs. According to Silvester et al., RTIL based on [NTf$_2$]$^-$ can form a stable protonated product [HNTF$_2$] in the HOR with a good electrochemical stability and a wide electrochemical potential window.[27,28] Meanwhile, compared with [Bmim][NTf$_2$], [Bmpy][NTf$_2$] has lower oxidation peak voltage, higher oxidation peak current, and higher hydrogen solubility, indicating that [Bmpy][NTf$_2$] has a more reasonable RTIL-electrode interface structure. CV needs to limit the gas diffusion velocity as much as possible to achieve diffusion-controlled conditions. At this time, the electrode reaction mainly depends on the HOR, which is beneficial to better explore the reaction mechanism. Due to the high viscosity of RTIL, it can be used as a diffusion barrier. Hydrogen dissolved and diffused in RTIL, followed by hydrogen adsorption and oxidation reactions at the three-phase interface. Finally, the hydrophobic polytetrafluoroethylene (PTFE) film was designed to block water vapor, which could cause cross-sensitive response to sensors. In addition, it could also allow air to flow smoothly when exposed to analyte gases. Due to the wide application of LIBs in life, transportation, aerospace, and other fields, it is necessary to detect hydrogen under aerobic and anaerobic conditions to ensure the safety of LIBs.

3.2.1. Sensing Properties under Anaerobic Conditions. CV was used to study the HOR mechanism under anaerobic conditions, and the scanning voltage range was set to −0.6−1.0 V. It is important to select a suitable scan rate that matches the gas flow rate for CV. When the scan rate decreases, the extent of the diffusion layer increases, the polarization current decreases accordingly, and the peak value of the CV curve becomes more prominent and obvious. However, the electrode reaction rate also decreases accordingly, which may cause the reaction to enter the reaction-controlled zone. Therefore, the selected scan rate was 20 mV/s during the CV. When the hydrogen concentration increases in turn, after completing the CVs under different hydrogen concentrations, the experimental data are shown in Figure 4a. The oxidation peak voltage was 0.35 V, reduction peak voltage was −0.4 V, and $E_{1/2}$ was −0.025 V, which was quite close to zero potential, as shown in Figure 4a.

https://doi.org/10.1021/acsomega.2c03610
ACS Omega 2022, 7, 24895−24902

It was also found that the oxidation peak voltage shifted to the right and the reduction peak voltage shifted to the left with the increase of hydrogen concentration, while the $E_{1/2}$ remained basically unchanged. When hydrogen concentration increased, a larger forward voltage was required correspondingly to ensure that the reaction rate was fast enough to deplete the hydrogen. The concentration of hydrogen and proton on the electrode surface was the same when $E = E_{1/2}$,[29] and the oxidation and reduction reaction rates reached a temporary balance. Then, the outward diffusion rate of proton was accelerated. It can be observed that when the hydrogen concentration was greater than 6000 ppm, the oxidation peak potential shifted to the right, and the reason for the left shift of the reduction peak was basically the same as that of the oxidation peak. In addition, the reduction peak current of the CV curve was found to be larger than the oxidation peak. WE is a Pt-loaded Ti foam and CE is a carbon electrode. Thus, the electrochemical activity of CE is much smaller than that of WE. When the CV was scanning, the generated protons cannot react completely and gradually accumulated. Furthermore, the accumulated protons in the negative CV scan all react on WE, resulting in the reduction reaction kinetics which was greater than that of the oxidation reaction. With the progress of each CV, the reduction current was increasing, leading to the unclosed curve. Within the range of 10 000 ppm, it indicated that the electrochemical reaction was under diffusion-controlled conditions. The linear fitting between the hydrogen concentration and the peak currents of oxidation and reduction reached 0.99 and 0.98, respectively, showing a good linear relationship, as shown in Figure 5a. However, considering the phenomenon of the right shift of the peak potential, the hydrogen concentration was adjusted to be less than 6000 ppm in the chronoamperometry process, which was more reliable.

It is well known that HOR in acidic aqueous electrolytes basically follows the Tafel−Volmer and Heyrovsky−Volmer pathways processes.[30] The steps of HOR of Ti-based Pt electrodes in RTIL are similar to the Tafel reaction, Volmer reaction, and Heyrovsky reaction.[31] Hydrogen was firstly adsorbed on the Pt surface to form Pt−$H_{(ad)}$, and Pt−$H_{(ad)}$ was oxidized to form a hydrogen radical (Pt−$H^{\bullet}$) and a proton (H^+) in the second step, which followed eqs 2−4

$$2Pt + H_2(g) \leftrightarrow 2Pt{-}H_{(ad)} \quad (2)$$

$$2Pt{-}H_{(ad)} \leftrightarrow Pt + Pt{-}H^{\bullet} + H^+ + e^- \quad (3)$$

$$Pt{-}H_{(ad)} \leftrightarrow Pt + H^+ + e^- \quad (4)$$

When performing chronoamperometry experiments, the performance and lifetime of the electrochemical sensor have a great dependence on the setting of potential. According to the oxidation peak potential obtained by CV, 0.5 V was selected as the bias voltage. The gas diffused simultaneously on both sides through Ti foam and porous ceramic and reached the three-phase interface directly, without the diffusion process in RTIL. The sensor package was designed with a vent, and a through gas diffusion path was formed during the sensor detection process, as shown in the layered device structure of Figure 1c. The sensitivity of the sensor reached 3.9 nA/ppm, and the T_{90} of the sensor was about 92 s (Figure 5b). The noise of the sensor was 4 nA, and the detection limit (LOD) was calculated to be 3.1 ppm based on a signal-to-noise ratio (SNR) of 3. In addition, the linear fitting value of hydrogen concentration and response current was 0.99, which had a good linear relationship (Figure 5b).

In fact, the reduction reaction rate on CE is independent of the oxidation reaction rate on WE. Because it was found that there is an open circuit between WE and CE, no charge transfer occurs. CE only acts to balance the voltage drop produced by the Faradaic current and reduce the oxidation products, so as to avoid excessive accumulation of the proton in RTIL in the HOR. In turn, the electrolyte will be damaged and the lifespan of the sensor will be shortened by excessive acidification for a long time. The protons released by WE need to diffuse in RTIL and migrate to CE for reduction reaction. However, WE and CE form a conducting loop in the traditional three-electrode principle of electrochemistry, and the reaction rates on WE and CE are consistent. Therefore, different from the traditional three-electrode principle in electrochemistry, the migration rate and reduction reaction rate of protons in RTIL of sensors under applied bias voltage do not limit the electrochemical reaction rate on WE.

3.2.2. Sensing Properties under Aerobic Conditions. Next, the mechanism of HOR under aerobic conditions was explored using CV. The scanning voltage range is −1.5 to 1.8 V, and the potential range is wider than that under anaerobic conditions. Therefore, the drying of RTIL and the removal of gaseous and water molecules are important, otherwise additional peaks may appear in the water electrolysis reaction at high potential. In the negative voltage sweep, oxygen is reduced and superoxide radical ($O_2^{\bullet-}$) is generated, unlike in anaerobic conditions, as shown in eq 5. During the positive voltage sweep, $O_2^{\bullet-}$ is oxidized and Pt−O is generated, which is seen in eq 6. The CV curve shows a reduction peak at −0.75 V and an oxidation peak at 0.3 V, which is shown in the results of CV in synthetic air in Figure 5a.

In addition, it could be observed that oxygen is consumed by HOR under aerobic conditions. The reason is that the current decreases at the oxidation peak at 0.3 V when exposed to hydrogen. At the same time, with the increase in hydrogen concentrations, the reduction current increases slightly around −1 V, suggesting that there is a coupled reaction between the hydrogen oxidation process and the oxygen reduction process. The higher the hydrogen concentration, the more $O_2^{\bullet-}$ that is consumed by HOR. Consequently, the oxygen reduction process is promoted according to eq 7. It can be seen that the mechanism of HOR is different from that under anaerobic conditions due to the participation of oxygen. The oxidation peak of HOR appears around 1.2 V, which is higher than the oxidation peak potential under anaerobic conditions. It shows that there is a good linear relationship between the peak current and gas concentration in the range of 5000 ppm. The linear fitting values between hydrogen concentration and the peak currents of oxidation and reduction of CV reached 0.99 and 0.98, respectively, as shown in Figure 5a. It is indicated that the electrochemical reaction is in the diffusion-controlled region in the hydrogen concentration range of 0−5000 ppm. The reaction mechanism is shown below, which was first proposed by Zeng[31]

$$O_2 + e^- \leftrightarrow O_2^{\bullet-} \quad (5)$$

$$2Pt + O_2^{\bullet-} - e^- \leftrightarrow 2Pt{-}O \quad (6)$$

$$2Pt + H_2 + 2O_2^{\bullet-} - e^- \leftrightarrow 2Pt{-}HO_2^{\bullet} \quad (7)$$

$$Pt{-}HO_2^{\bullet} - e^- \leftrightarrow Pt + O_2 + H^+ \quad (8)$$

https://doi.org/10.1021/acsomega.2c03610
ACS Omega 2022, 7, 24895−24902

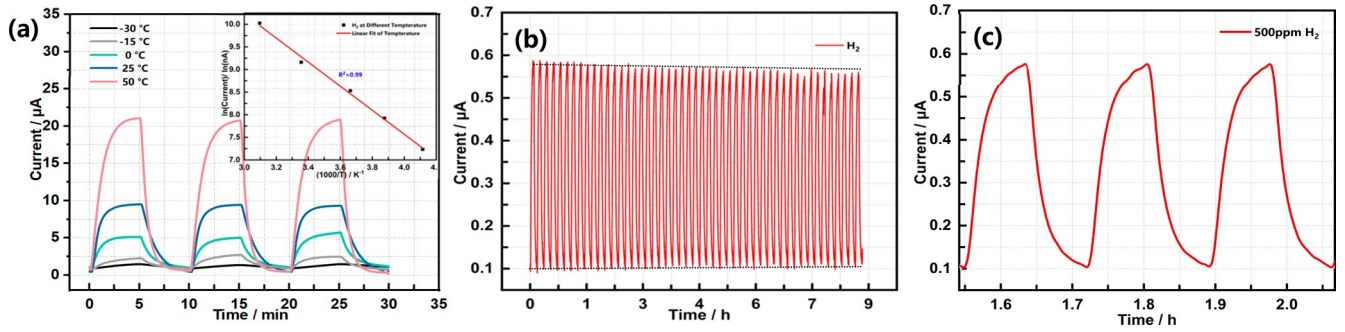

Figure 6. (a) Sensing performance under different temperature conditions, with the linear fit of the response current in the inset, (b) prolonged continuous operation (48 cycles within 8 h), and (c) magnified images of three of the response stages in part b.

$$Pt{-}HO_2^{\bullet} + H^+ + e^- \leftrightarrow Pt + H_2O_2 \quad (9)$$

The chronoamperometry experiment was performed in aerobic conditions with a bias voltage of 1 V which was based on the oxidation peak potential of the HOR by CV (Figure 5a). It was found that the current of the HOR under aerobic conditions was smaller and the sensitivity was lower than that in the anaerobic environment. The sensitivity of the sensor was 0.9 nA/ppm, the T_{90} was 84 s, the noise was 3 nA, and LOD was 6.6 ppm, as shown in the results of Figure 5b. The electrochemical reaction under diffusion-controlled conditions was also illustrated in the hydrogen concentration range of 5000 ppm. The linear fit of the current under different oxygen concentrations reached about 0.99. At the same time, it was found that there was another mechanism of HOR in addition to eqs 5−9 in aerobic conditions. It can be observed that the baseline current continuously moved down with the increase of hydrogen concentration, as shown in Figure 5b. The product ($Pt{-}HO_2^{\bullet}$) of the coupling reaction of the hydrogen oxidation process and the oxygen reduction process could continue to participate in the oxidation or reduction reaction.[31] Equation 3 indicated that the protons were also generated at the same time as the hydrogen radical intermediate ($Pt{-}H^{\bullet}$). The kinetics of the reduction reaction of $Pt{-}HO_2^{\bullet}$ was greatly enhanced due to the accumulation of protons after the hydrogen response phase, as shown in eq 9, which led to a partial cancellation of the positive background current in the equilibrium phase. It is even foreseeable that if the hydrogen concentration is increased, the background current may become negative. Therefore, electrochemical gas sensors are not suitable for detecting high concentrations of hydrogen in aerobic conditions and should be avoided, as reported for common electrochemical gas sensors.[31]

Furthermore, the tolerance of temperature on the sensor performance was investigated. A series of temperatures were controlled within the range of 243−323 K, and the output current of the sensor was detected under the same hydrogen concentration (2000 ppm). When the temperature was lower than 243 K, the sensor lost response due to the limited mass transfer process and the extremely slow reaction rate. At lower temperatures (243−273 K), both the response speed and the sensitivity of the sensor become smaller, the background current is larger, as shown in Figure 6a. It showed that the hydrogen dissolved in RTIL was not completely reacted due to the slow rate of HOR. When the temperature between 273 and 323 K, the background current is significantly reduced and better sensitivity is achieved. Above 323 K, the electrical connection degraded and the sensor output became unstable. The accumulation of excess reaction by-products in the electrolyte film can lead to changes in the electrical properties, such as conductivity or acidity. As a result, the sensitivity of the sensor changes and the signal of sensor becomes unreliable. In severe cases, it will directly deplete the electrolyte and reduce the life of the sensor.[32] The relationship between the temperature of the electrochemical sensor and the output current conforms to the Arrhenius formula,[33] as shown in eq 10

$$k = B\, e^{-E_a/RT} \quad (10)$$

Here, k is the rate constant, R is the molar gas constant, T is the thermodynamic temperature, E_a is the apparent activation energy, and B is the frequency factor. It is also indicated that the sensor can work normally in the temperature range of 243−323 K. The response at each temperature was fitted, and the linearity was found to be 0.99, as shown in Figure 6a. In addition, it shows that the stability and repeatability of the sensor meet the standards. The transient response to hydrogen (300 ppm balanced with N_2) was repeated for 8 h as given in Figure 6b. It was found that the response of the sensor decreased a bit during the test. The reason is speculated to be the slight accumulation of protons during long-term testing according to the electrochemical behavior of hydrogen mentioned above, which in turn leads to a slight decrease in the HOR kinetics of WE. Overall, one could find that both the base and responding currents have a very small drift less than 0.3 nA for a long time, which indicates our sensors have a very good stability and reproducibility.

Finally, the sandwich device structure scheme provides a good idea for the development of high-performance electrochemical gas sensors and is also applicable to other porous electrode materials. Two different materials, nickel foam (Ni foam) and copper foam (Cu foam), were used to load Pt. The characterization of the materials and the exploration of the electrochemical behavior of hydrogen are shown in Figure S4. The feasibility of different electrode materials for electrochemical hydrogen sensors is preliminarily shown. It also reflects the potential research value of the sandwich device structure.

CONCLUSION

In summary, we proposed an electrochemical gas sensor design with a "sandwich" structure of Pt-NPs-supported metal foam and SPE electrodes based on porous substrates. The solid polymer electrolyte was innovatively filled into the porous WE, which optimizes the gas diffusion path and effectively improves the sensitivity and response speed of the sensor. The HOR

https://doi.org/10.1021/acsomega.2c03610
ACS Omega 2022, 7, 24895−24902

mechanism of the Pt-loaded Ti foam electrode under both anaerobic and aerobic conditions was fully discussed, and the high performance of the sensor was demonstrated. The development of the sensor provides a commercial idea for the safe real-time monitoring of LIBs. In the next step, the potentiostatic hydrogen detector will conduct larger-scale experiments in a practical application environment and extend the "sandwich" device structure to a wider range of detection of different kinds of gases.

■ ASSOCIATED CONTENT

Supporting Information

The Supporting Information is available free of charge at https://pubs.acs.org/doi/10.1021/acsomega.2c03610.

Experimental methods, experimental setup, analysis of electroplating, and extension of the structure (PDF)

■ AUTHOR INFORMATION

Corresponding Authors

Shurui Fan − *Tianjin Key Laboratory of Electronic Materials and Devices, School of Electronic and Information Engineering, Hebei University of Technology, Tianjin 300401, China*; Email: fansr@hebut.edu.cn

Zhongqiu Hua − *Tianjin Key Laboratory of Electronic Materials and Devices, School of Electronic and Information Engineering, Hebei University of Technology, Tianjin 300401, China*; orcid.org/0000-0002-6461-7910; Email: zhongqiuhua@hebut.edu.cn

Authors

Wanshuo Gao − *Tianjin Key Laboratory of Electronic Materials and Devices, School of Electronic and Information Engineering, Hebei University of Technology, Tianjin 300401, China*

Zinan Zhi − *Tianjin Key Laboratory of Electronic Materials and Devices, School of Electronic and Information Engineering, Hebei University of Technology, Tianjin 300401, China*

Haoyi Li − *Tianjin Key Laboratory of Electronic Materials and Devices, School of Electronic and Information Engineering, Hebei University of Technology, Tianjin 300401, China*

Xuanyue Pan − *Tianjin Key Laboratory of Electronic Materials and Devices, School of Electronic and Information Engineering, Hebei University of Technology, Tianjin 300401, China*

Wentao Sun − *Tianjin Key Laboratory of Electronic Materials and Devices, School of Electronic and Information Engineering, Hebei University of Technology, Tianjin 300401, China*

Huicheng Gao − *Tianjin Key Laboratory of Electronic Materials and Devices, School of Electronic and Information Engineering, Hebei University of Technology, Tianjin 300401, China*

Complete contact information is available at: https://pubs.acs.org/10.1021/acsomega.2c03610

Author Contributions

†W.G. and Z.Z. contributed equally. The manuscript was written through the contributions of all authors. All authors have given approval to the final version of the manuscript.

Notes

The authors declare no competing financial interest.

■ ACKNOWLEDGMENTS

This study was supported by National Natural Science Foundation of China (Grant No. 42075129). The characterization results were supported by Beijing Zhongkebaice Technology Service Co., Ltd.

■ REFERENCES

(1) Sun, Y.; Liu, N.; Cui, Y. Promises and challenges of nanomaterials for lithium-based rechargeable batteries. *Nature Energy* **2016**, *1*, 16071.

(2) Chu, S.; Cui, Y.; Liu, N. The path towards sustainable energy. *Nature Materials* **2017**, *16*, 16−22.

(3) Wang, Q.; Sun, J.; Yao, X.; Chen, C. Thermal stability of $LiPF_6$/EC+DEC electrolyte with charged electrodes for lithium ion batteries. *Thermochimica Acta* **2005**, *437* (1-2), 12−16.

(4) Yang, Z.; Zhang, J.; Kintner-Meyer, M.; Lu, X.; Choi, D.; Lemmon, J. P.; Liu, J. Electrochemical energy storage for green grid. *Chem. Rev.* **2011**, *111* (5), 3577−3613.

(5) Feng, X.; Fang, M.; He, X.; Ouyang, M.; Lu, L.; Wang, H.; Zhang, M. Thermal runaway features of large format prismatic lithium ion battery using extended volume accelerating rate calorimetry. *J. Power Sources* **2014**, *255*, 294−301.

(6) Bugryniec, P. J.; Davidson, J. N.; Brown, S. F. Assessment of thermal runaway in commercial lithium iron phosphate cells due to overheating in an oven test. *Energy Procedia* **2018**, *151*, 74−78.

(7) Du Pasquier, A.; Disma, F.; Bowmer, T.; Gozdz, A. S.; Amatucci, G.; Tarascon, J.-M. Differential scanning calorimetry study of the reactivity of carbon anodes in plastic Li-ion batteries. *J. Electrochem. Soc.* **1998**, *145* (2), 472−477.

(8) Wang, H.; Tang, A.; Wang, K. Thermal Behavior Investigation of $LiNi_{1/3}CO_{1/3}Mn_{1/3}O_2$-Based Li-ion Battery under Overcharged Test. *Chin. J. Chem.* **2011**, *29* (1), 27−32.

(9) Yuan, L.; Dubaniewicz, T.; Zlochower, I.; Thomas, R.; Rayyan, N. Experimental study on thermal runaway and vented gases of lithium-ion cells. *Process Safety and Environmental Protection* **2020**, *144*, 186−192.

(10) Jin, Y.; Zheng, Z.; Wei, D.; Jiang, X.; Lu, H.; Sun, L.; Tao, F.; Guo, D.; Liu, Y.; Gao, J.; Cui, Y. Detection of Micro-Scale Li Dendrite via H2 Gas Capture for Early Safety Warning. *Joule* **2020**, *4* (8), 1714−1729.

(11) Baltes, N.; Beyle, F.; Freiner, S.; Geier, F.; Joos, M.; Pinkwart, K.; Rabenecker, P. Trace detection of oxygen − ionic liquids in gas sensor design. *Talanta* **2013**, *116*, 474−481.

(12) Lee, J.; Hussain, G.; López-Salas, N.; MacFarlane, D. R.; Silvester, D. S. Thin films of poly(vinylidene fluoride-co-hexafluoropropylene)-ionic liquid mixtures as amperometric gas sensing materials for oxygen and ammonia. *Analyst* **2020**, *145* (5), 1915−1924.

(13) Liu, X.; Chen, X.; Xu, Y.; Zeng, X. Platinum−Nickel Bimetallic Nanosphere−Ionic Liquid Interface for Electrochemical Oxygen and Hydrogen Sensing. *ECS Meeting Abstracts* **2021**, *MA2021-01* (63), 1703−1703.

(14) Buttner, W. J.; Post, M. B.; Burgess, R.; Rivkin, C. An overview of hydrogen safety sensors and requirements. *International Journal of Hydrogen Energy* **2011**, *36* (3), 2462−2470.

(15) Staffell, I.; Scamman, D.; Velazquez Abad, A.; Balcombe, P.; Dodds, P. E.; Ekins, P.; Shah, N.; Ward, K. R. The role of hydrogen and fuel cells in the global energy system. *Energy Environ. Sci.* **2019**, *12* (2), 463−491.

(16) Soundarrajan, P.; Schweighardt, F. Hydrogen Sensing and Detection. In *Hydrogen Fuel*, 1st ed.; CRC Press, 2008; pp 495−534.

(17) Hübert, T.; Boon-Brett, L.; Black, G.; Banach, U. Hydrogen sensors − A review. *Sens. Actuators, B* **2011**, *157* (2), 329−352.

(18) Brosha, E. L.; Romero, C. J.; Poppe, D.; Williamson, T. L.; Kreller, C. R.; Mukundan, R.; Glass, R. S.; Wu, A. S. Editors'

Choice—Field Trials Testing of Mixed Potential Electrochemical Hydrogen Safety Sensors at Commercial California Hydrogen Filling Stations. *J. Electrochem. Soc.* **2017**, *164* (13), B681−B689.
(19) Stetter, J. R.; Sedlak, J. M.; Blurton, K. F. Electrochemical gas chromatographic detection of hydrogen sulfide at PPM and PPB levels. *Journal of Chromatographic Science* **1977**, *15* (3-4), 125−128.
(20) Silvester, D. S. New innovations in ionic liquid−based miniaturised amperometric gas sensors. *Current Opinion in Electrochemistry* **2019**, *15*, 7−17.
(21) Gao, J.; Hua, Z.; Xu, S.; Wan, H.; Zhi, Z.; Chen, X.; Fan, S. Amperometric gas sensors based on screen printed electrodes with porous ceramic substrates. *Sensors and Actuators B: Chemical* **2021**, *342*, 130045.
(22) Korotcenkov, G.; Han, S. D.; Stetter, J. R. Review of Electrochemical Hydrogen Sensors. *Chem. Rev.* **2009**, *109* (3), 1402−1433.
(23) Blurton, K. F.; Stetter, J. R. Sensitive electrochemical detector for gas chromatography. *Journal of Chromatography A* **1978**, *155* (1), 35−45.
(24) Wang, R.; Wu, P.; Zhi, Z.; Gao, W.; Hua, Z. Amperometric hydrogen sensor based on pyrrolidinium hydrogen sulfate under anaerobic conditions. *Chinese Journal of Analytical Chemistry* **2022**, DOI: 10.1016/j.cjac.2022.100065.
(25) Trasatti, S.; Petrii, O. A. Real surface area measurements in electrochemistry. *Pure & Applied Chemistry* **1991**, *63* (5), 711−734.
(26) Li, W.; Lane, A. M. Resolving the HUPD and HOPD by DEMS to determine the ECSA of Pt electrodes in PEM fuel cells. *Electrochemistry Communications* **2011**, *13* (9), 913−916.
(27) Silvester, D. S.; Aldous, L.; Hardacre, C.; Compton, R. G. An Electrochemical Study of the Oxidation of Hydrogen at Platinum Electrodes in Several Room Temperature Ionic Liquids †. *J. Phys. Chem. B* **2007**, *111* (18), 5000−5007.
(28) Silvester, D. S.; Ward, K. R.; Aldous, L.; Hardacre, C.; Compton, R. G. The electrochemical oxidation of hydrogen at activated platinum electrodes in room temperature ionic liquids as solvents. *Journal of Electroanalytical Chemistry* **2008**, *618* (1-2), 53−60.
(29) Elgrishi, N.; Rountree, K. J.; McCarthy, B. D.; Rountree, E. S.; Eisenhart, T. T.; Dempsey, J. L. A Practical Beginner's Guide to Cyclic Voltammetry. *Journal of Chemical Education* **2018**, *95* (2), 197−206.
(30) Cleghorn, S. J.; Ren, X.; Springer, T. E.; Wilson, M. S.; Zawodzinski, C. PEM fuel cells for transportation and stationary power generation applications. *Int. J. Hydrogen Energy* **1997**, *22*, 1137−1144.
(31) Wang, Z.; Zeng, X. Bis(trifluoromethylsulfonyl)imide (NTf_2)-Based Ionic Liquids for Facile Methane Electro-Oxidation on Pt. *J. Electrochem. Soc.* **2013**, *160* (9), H604−H611.
(32) Kuberský, P.; Syrový, T.; Hamáček, A.; Nešpůrek, S.; Syrová, L. Towards a fully printed electrochemical NO_2 sensor on a flexible substrate using ionic liquid based polymer electrolyte. *Sens. Actuators, B* **2015**, *209*, 1084−1090.
(33) Nádherná, M.; Opekar, F.; Reiter, J.; Štulík, K. A planar, solid-state amperometric sensor for nitrogen dioxide, employing an ionic liquid electrolyte contained in a polymeric matrix. *Sens. Actuators, B* **2012**, *161* (1), 811−817.

https://doi.org/10.1021/acsomega.2c03610
ACS Omega 2022, 7, 24895−24902